Research Article

Fabrication of novel $CuWO_4$ nanoparticles (NPs) for photocatalytic degradation of methylene blue in aqueous solution

Xiaolin Hu[1] · Di Gao[1] · Yanhong Li[2] · Hongmei Dong[1] · Wen Zhou[1] · Lin Yang[2] · Yunhuai Zhang[1]

Abstract
In this paper, the UV–Vis photocatalytic degradation of methylene blue (MB) by copper tungstate ($CuWO_4$) has been studied in neutral aqueous heterogeneous suspensions $CuWO_4$ nanochains and nanoparticles were synthesized via solvothermal method. $CuWO_4$ was evaluated regarding a photocatalytic degradation of organic dyes, which is highly important to decontaminate water. Our results demonstrate that the $CuWO_4$ nanoparticles have a better photocatalytic degradation performance than nanochains, and the nanoparticles with 86% of MB degradation is obtained after 90 min UV–Vis irradiation. Further, the MB degradation process follows Langmuir–Hinshelwood mechanism first order kinetics, in the process of MB degradation, O_2^- and ·OH acted as the main reactive species. This work provides an overall strategy for further study on the catalysts for photo degradation of organic pollutant.

Keywords $CuWO_4$ · Photocatalytic degradation · Mechanism · Decolourization ratio · Water purification

1 Introduction

Today, environmental pollution is a global issue, especially water pollution is a key problem. The textile industry is one of the most polluted industrial sectors and also a large amount of water for consumers. Textile wastewater usually includes of dyes, surfactants, minerals, heavy spiritual ions, detergents, electrolytes, solvents and stubborn compounds. Dye is the main source in textile wastewater, it affects the color of wastewater and reduces the transmission of light through expansion [1–4]. Water pollution is an acute and chronic effect on human health, affecting many different systems. Then, it is urgent to solve the problem of water pollution. No classified treatment of the organic pollution caused by treating wastewater indiscriminately is a worldwide environmental problem, which is very harmful to human health [5]. Therefore, it is an essential to find out an environment-friendly green technology which has a potential to improve environment. Recent days, different technical approaches such as ion exchange, electrochemical reactions, oxidation, adsorption and reduction have been referred for the removal of these pollutants from the industrial waste water [6]. In these methods, the photocatalytic degradation of organic pollutants by semiconductors is being paid more and more attention, which is the preferred method for the degradation of organic waste because it is efficient and cheap. In semiconductor photocatalysis, when material is exposed to photo radiation electron pair. Electrons enter the conduction band by creating holes in the valence band and reacting with pollutants through oxidation and reduction. Therefore, photocatalysts must be photosensitive, chemically stable, absorbing the maximum solar radiation, non-toxic and economical [7].

The significant energy percentage of the solar radiation (43%) corresponds to visible light. As a result, researchers have recently been interested in photocatalysts ultraviolet–visible–light–driven [8]. The development of new and more effective ultraviolet visible light driven photocatalyst has been still an important topic of solar energy utilization.

✉ Yunhuai Zhang, xp2031@163.com | [1]College of Chemistry and Chemical Engineering, Chongqing University, Chongqing 400044, China. [2]College of Physics, Chongqing University, Chongqing 400044, China.

SN Applied Sciences (2019) 1:119 | https://doi.org/10.1007/s42452-018-0113-9

Received: 4 September 2018 / Accepted: 7 December 2018 / Published online: 20 December 2018

$CuWO_4$ is a promising material for solar oxidation that has received attention. Moreover, the degradation of contaminants in aqueous solution by $CuWO_4$ nanochains has not been studied. The monoclinic structure of the wolframite type is common to the tungstate consisting of transition metals. The transition mental belongs to the fourth period of the periodic table ($ZnWO_4$ [9], $NiWO_4$ [10], $CoWO_4$ [11], $FeWO_4$ [12], and $MnWO_4$ [13]. The only exception is $CuWO_4$, which crystallizes at room temperature with a triclinic structure [14, 15]. In addition, the $CuWO_4$ crystals with triclinic structure is affected by second-order Jahn–Teller (SOJT) effect. $CuWO_4$ is a n-type semiconductor with an indirect band gap of 2.25 eV [16]. The band gap strongly depends on the structure of WO_6 and CuO_6 octahedra and how they are coupled [17, 18]. Research has shown that traditional binary metal oxide semiconductor has good photocatalytic stability. In addition, binary metallic oxide has the great potential in this aspect. The Cu ($3d^{22}_{x-y}$) and O (2p) hybridization orbit feature can effectively reduce the band gap of the material and extend absorption range. Moreover, the method of increasing the valence band in the formation of the ternary mental oxide is better than the reducing the location of semiconductor conduction band in order to reduce the band gap. Tungsten ions have a formal +6 valence state ($5d^0$ electron configuration), forming partial covalent bonds and six oxygen atoms. As a result, the octahedron of WO_6 is distorted by the second-order SOJT effect. There configuration improves the absorption capacity of visible light and photocatalytic stability [19–23].

Due to the toxicity of MB, water and water waste have attracted significant attention in the green environment. In this contribution, we use the $CuWO_4$ to investigate the photocatalytic degradation of organic pollutants MB performance in water solution by UV–Vis. The photocatalytic materials are including the nanoparticles and nanochains assembled from nanoparticles, the two type samples were synthesized though a solvothermal method. Additionally, the mechanism of photocatalytic degradation was analyzed by kinetic and photogenic electron hole.

2 Experimental

2.1 Materials

Copper (II) chloride dihydrate ($CuCl_2{\cdot}2H_2O$), tungstate (VI) sodium dehydrate ($Na_2WO_4{\cdot}2H_2O$), copper (II) nitratetrihydrat ($Cu(NO_3)_2{\cdot}3H_2O$), sodium bromide (NaBr), polyvinyl pyrrolidone (PVP), trisodium citrate ($C_6H_5O_7Na_3{\cdot}2H_2O$), methylene blue (MB), ethylene glycol (EG) and ethanol were all obtained from Chuan Dong Ltd. All of these reagents were analytical grade and were used without further purification. Deionized (DI) water (18.2 MΩ cm) was used in the whole experiment.

2.2 Preparation of $CuWO_4$ nanochains

$CuWO_4$ nanochains was synthesized via solvothermal method as follows. Firstly, 1 mmol of $Cu(NO_3)_2{\cdot}3H_2O$ and 1 mmol $Na_2WO_4{\cdot}2H_2O$ were dissolved into a mixture of 15 mL of ethylene glycol and 5 mL of DI water. 5 mmol of $C_6H_5O_7Na_3{\cdot}2H_2O$ and 1 mmol of NaBr were added into the as-prepared mixture solution under magnetic stirring. Then the green solution was magnetically stirred for 60 min at room temperature completely dissolved to a homogeneous solution and was transferred into a glass bottle. That were both transferred into 50 mL Teflon lined stainless steel autoclave and maintained at 170 °C for 12 h. After cooling to the room temperature, the resulting brick-red sediments were washed with anhydrous ethanol and DI water for several times to remove the surfactant and then dried at 60 °C in air for 8 h. After drying, the solid powders were annealed at 500 °C for 3.5 h at the heating rate of 2 °C/min under air atmosphere.

2.3 Preparation of $CuWO_4$ nanoparticles

For the facile solvothermal method synthesis of $CuWO_4$ nanoparticles, the standard synthesis process is as follows: firstly, 8 mmol of $Na_2WO_4{\cdot}2H_2O$ and 8 mmol of $CuCl_2{\cdot}2H_2O$ were dissolved in 160 ml pure solvent of ethylene glycol. Then the blue solution was magnetically stirred at room temperature for 60 min and a certain amount of PVP was added into the above as-prepared solution. The above mixture was then stirred for 30 min, and the homogeneous blue-white precursor solution was transferred into the polytetrafluoroethylene lined stainless steel autoclave and heated at 170 °C for 12 h. After cooling to room temperature, the products were washed with DI water and hydrous ethanol several times, respectively, and then dried at 60 °C in air for 8 h. Finally, the powders were sintered in air at 500 °C for 3.5 h at a heating rate of 2 °C/min.

2.4 Characterization instruments

The powder XRD system (PXRD, Shimadzu ZD-3AX) equipped with Cu Kα radiation source (λ = 1.5406 Å) were studied in order to identify the crystallography of as-synthesized nanomaterials, 2 θ rang of 10°–70° with 5° and a step time of 1 min is used to collect the data. Fourier transform infrared (FTIR) spectra were performed using a Nicolet 6700 FTIR spectrophotometer in the range of 400–4000 cm^{-1} by a KBr pellet method with ratio of 1:100 for samples to KBr. The Brunauer–Emmett–Teller (BET) surface area was measured by the nitrogen adsorption isotherms measurements

(Micromeritics ASAP 2020). The surface morphology was analyzed by scanning electron microscopy (FE-SEM, Nova 400 Nano-SEM). The UV–Vis absorption spectrophotometer (TU-1810SPC) was used to study the optical properties of all the samples in the spectral range of 200–800 nm.

2.5 Photocatalytic measurements

Photocatalytic activities of the $CuWO_4$ nanoparticles and nanochains were evaluated by the photocatalytic degradation of MB neutral solutions. Experiments were conducted as follows: firstly, 10 mg of the MB were dispersed in 100 mL DI water and then put it in a 1000 mL volumetric flask, the 100 mL MB aqueous solution was taken out and placed in the beaker and covered with a black cloth. Subsequently, 40 mg of photocatalyst was added to 10 mg/L MB aqueous solution under ultrasonication for 10 min at room temperature until the homogeneous solution was formed. Before lighting, the mixed suspension was stirred in the dark for 60 min to achieve the adsorption–desorption equilibrium between the photocatalyst and MB. Then the stirred suspension was illuminated by a 300 W Xenon lamp (PLS-SXE300UV) as light source. At 10 min irradiation time intervals, after irradiation, 2 mL of suspensions were collected, the concentration of the reaction solution was determined by ultraviolet visible spectrophotometer and the absorption peak was measured at 664 nm. The total reaction time was 90 min, and the UV–Vis adsorption spectrum was recorded in the region of 200–800 nm.

The degradation efficiency (%) was calculated on the basis of the Eq. 1 as follow:

$$\text{degradation}\,(\%) = \frac{C_0 - C}{C_0} \times 100\% \quad (1)$$

where C_0 is the initial concentration of MB after adsorption, and the desorption equilibrium is achieved before irradiation. C is the concentration of pollutants in different time intervals after photocatalytic reaction. In the absence of a catalyst, a blank test was conducted to assess the role of catalyst in the degradation process.

The efficiency of this degradation and the kinetic rate of MB dye degradation was computed in the presence of the synthesized $CuWO_4$ nanoparticles and nanochains assembled from nanoparticles.

3 Results and discussion

3.1 Characterization of the synthesized $CuWO_4$ with nanochains and nanoparticles

The typical XRD patterns of $CuWO_4$ with nanochains and nanoparticles morphologies were synthesized via solvothermal method as shown in Fig. 1a. It is obvious that the powder diffraction pattern could be assigned to the pure phase of $CuWO_4$ (JCPDS No. 72-0616), which are consistent with the pure $CuWO_4$ phase (ICSD card No.16009) [24]. According to this figure, there are several peaks at 2 θ of 19 [100], 22.9 [110], 23.6 [0–11], 24.1 [011], 26.9 [101], 28.7 [–1–11], 30.1 [111], 36.4 [021], 38.6 [–120]. All the peaks in the XRD spectra are completely matched with the pure $CuWO_4$ phase, and there are no obvious peaks resulting from impurities, such as copper oxide or tungstic oxide were discovered, proving that the triclinic phase is $CuWO_4$. In order to confirm the triclinic structure of $CuWO_4$ crystals, the structure of periodic or ordered $CuWO_4$ crystal was refined by means of Rietveld method [25]. The refinement of the $CuWO_4$ crystal is shown in Fig. 1b. The structure refinement data (Table 1) shows that the $CuWO_4$ crystal

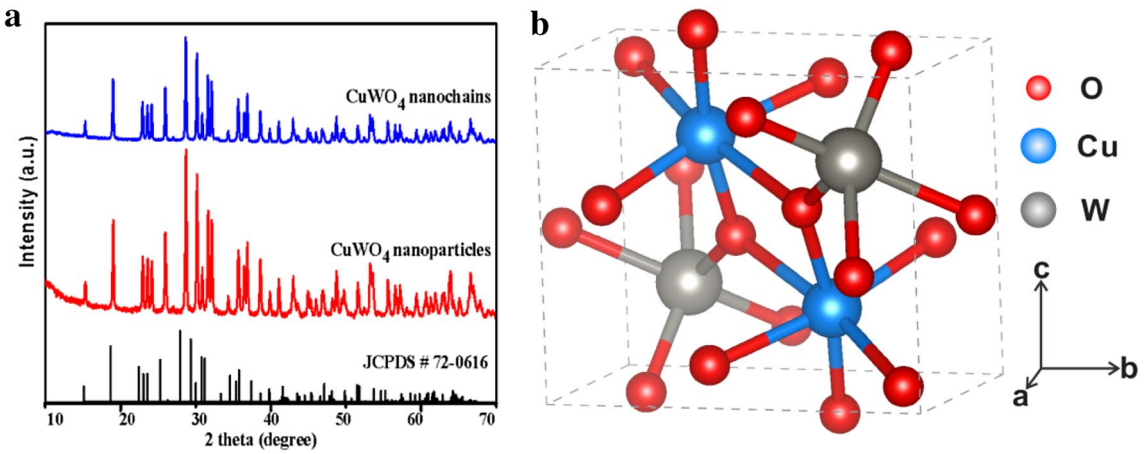

Fig. 1 **a** PXRD patterns of $CuWO_4$ crystals with different morphologies and **b** schematic illustration of a triclinic $CuWO_4$ unit cell indicating the distorted octahedral CuO_6 and WO_6 clusters

Table 1 The refined data from Rietveld are the lattice parameters, unit cell volume, atomic coordinates and site occupation of $CuWO_4$ crystal

Atoms	Wyck.	Site	a/x	b/y	c/z
Cu1	2i	1	16 (0.49533)	13 (0.65976)	15 (0.24481)
W1	2i	1	4 (0.02106)	3 (0.17348)	4 (0.25429)
O1	2i	1	10 (0.2491)	8 (0.3535)	10 (0.4245)
O2	2i	1	10 (0.2145)	7 (0.8812)	9 (0.4309)
O3	2i	1	10 (0.7353)	8 (0.3803)	9 (0.0981)
O4	2i	1	9 (0.7826)	8 (0.9097)	9 (0.053)

Cell: α = 91.677 (9)°, β = 92.469 (7)°, γ = 82.805 (10)°, a = 4.7026 (6) Å, b = 5.8389 (7) Å, c = 4.8784 (6) Å, v = 132.73 (3) Å, Z = 2

has a triclinic structure with a point group (C_i), space group ($P\bar{1}$, No.16009) and a molecular unit of two unit cell (Z = 2) [26]. The atomic position get from the Rietveld refinement data are illustrated in Table 1. The model describes the configuration of O–W–O and O–Cu–O bonds between [WO_6] and [CuO_6] clusters as a distorted octahedral structure. These clusters are made up of octahedron-type polyhedrons with twelve-sides, eight-faces and six-vertices, the distorted clusters play an important role in the formation of oxidant groups ·OH and $\cdot O_2^-$ radicals [27].

The $CuWO_4$ nanochains and nanoparticles were further analyzed by FT-IR spectra. As is shown in Fig. 2a, b, the absorption peaks near 3424 cm^{-1} is called the antisymmetric/symmetric vibration of the free water molecules adsorbed on the surface of the prepared material, and the peak of the 1632 cm^{-1} is the OH expansion vibration of the free hydrogen bond hydroxyl radical. Seven peaks (at 480, 561, 627, 723, 808, 912 and 1385 cm^{-1}) can be observed, which can be attributed to the tensile band and vibration of the $CuWO_4$ [28]. In the WO_4 structure, the infrared absorption peak at 480, 627 and 912 cm^{-1} might be due to the tensile mode of W–O. The small band at 808 cm^{-1} verified the stretching mode of the W–O-W bond. In the scope of 800–700 cm^{-1}, the features of the belt are Cu–O stretching vibration [29, 30]. Besides, we compared the variation in surface area of the $CuWO_4$ nanochains and nanoparticles. As is shown in Fig. 3a, b, the nitrogen adsorption–desorption isotherm shows that the Brunauer–Emmett–Teller (BET) surface area of $CuWO_4$ nanochains is 4.742 m^2/g, $CuWO_4$ nanoparticles is 10.832 m^2/g.

The morphology of the as-prepared $CuWO_4$ nanochains and nanoparticles were characterized by SEM microcopy, as shown in Fig. 4a, b, the magnified image is inserted in the lower left corner. From SEM images it is revealed that the surface morphology, interestingly, Fig. 4a shows that the $CuWO_4$ nanochains microcrystals are self-assembled by aggregated nanoparticles and the size of $CuWO_4$ nanoparticles (Fig. 4b) is in the range of 20–70 nm.

3.2 Photocatalytic activity and spectral characteristics

Photocatalytic activity of products under UV–Vis light irradiation was evaluated by photocatalytic degradation method, and the adsorption kinetics and adsorption equilibrium of $CuWO_4$ suspension were studied. In the dark, the adsorption equilibrium was established only for an hour. The maximum coverage of the surface was found to depend on the surface active sites, the chance of atomic collisions, and ultraviolet light exposure. The kinetic of adsorption is described by pseudo second order rate law. Figure 5a illustrates the absorption spectra of the MB

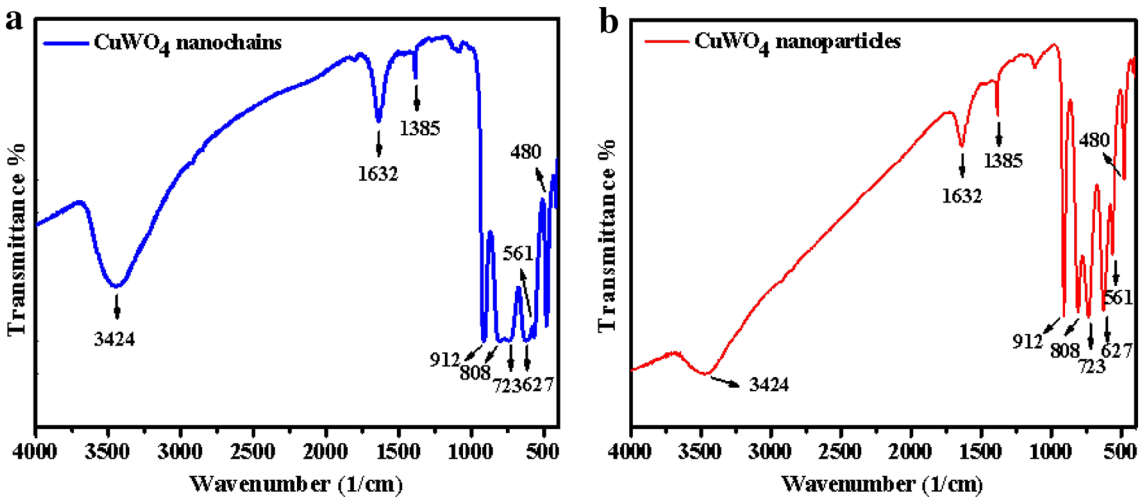

Fig. 2 FTIR spectrum of $CuWO_4$ nanocrystals **a** nanochains and **b** nanoparticles (the band of 808 and 723 cm^{-1} corresponds to the stretching vibration of W–O–W and Cu–O, respectively)

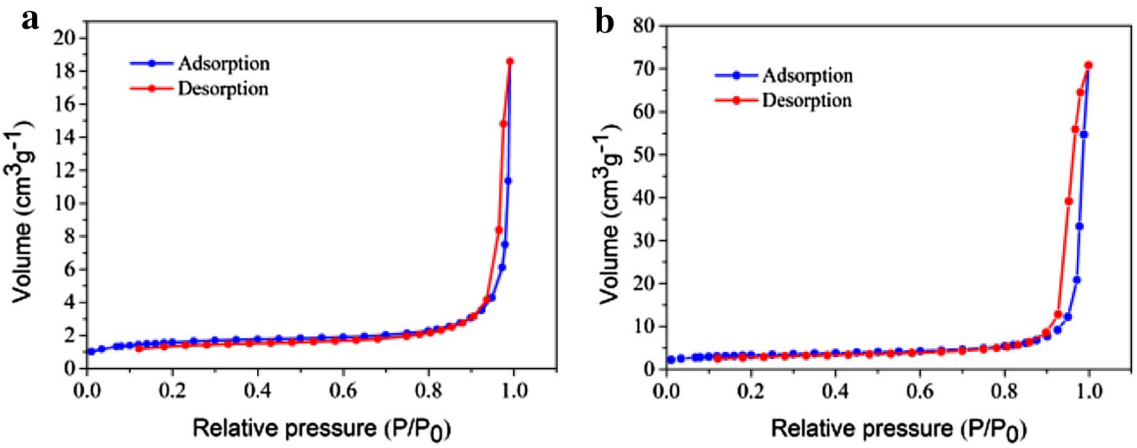

Fig. 3 Nitrogen adsorption—desorption isotherm **a** nanochains and **b** nanoparticles

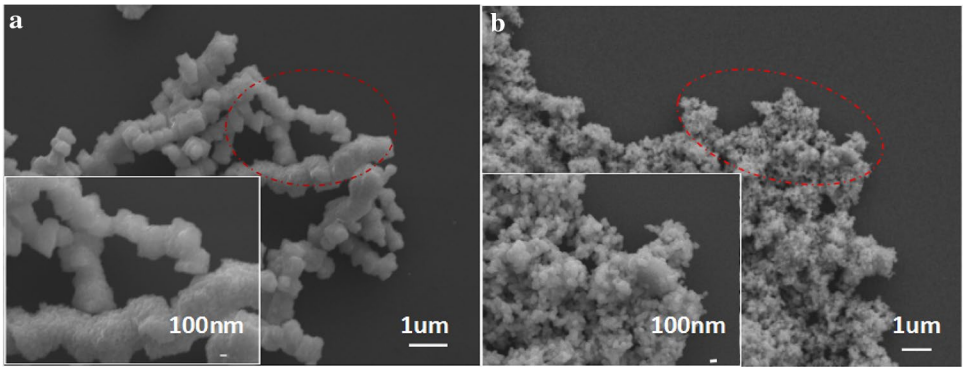

Fig. 4 SEM images of $CuWO_4$ samples **a** nanochains and **b** nanoparticles

solution in the absence of the catalyst taken at different degradation times under ultraviolet visible light irradiation. It can be seen that the autocatalysis of MB is negligible without $CuWO_4$ catalyst. Figure 5b, c are the temporal evolution of spectra by the 40 mg $CuWO_4$ nanochains and nanoparticles, which represent the photo degradation of 10 mg/L 100 mL MB under UV–Vis light illumination. Obviously, the absorption peaks for both samples at 664 nm corresponding to MB gradually become weaker, which is confirmed by the faded color of MB solution (Fig. 5d). Moreover, for $CuWO_4$ nanoparticles, the time-dependent spectra exhibit lower peak intensity than that of $CuWO_4$ nanochains, implying its better photo degradation activity of MB. In Fig. 5d, the curves of C/C_0 versus irradiation time and time-dependent photographs of MB solution are shown. For the $CuWO_4$ nanochains photocatalytic system, about 49% of MB was decomposed after 90 min irradiation. It is worth noting that for the photocatalytic system of $CuWO_4$ nanoparticles, about 86% of MB was decomposed after irradiation 90 min.

The physicochemical process of adsorption involves the transfer of MB dyes from liquid phase to the nanomaterial catalyst. In addition, the evaluation of reaction kinetics is the basis for the comparison of catalytic performance, kinetic analysis can be used to prove the effectiveness of the proposed mechanism. The study of the kinetics of the absorption process at different time periods provides a way of thinking for the mechanism of adsorption. For a quantitative understanding of the reaction kinetics of MB degradation, the kinetic curve of photocatalytic degradation has been studied by the simplified Langmuir–Hinshlwood (L–H) kinetics, which is well confirmed on the low concentration of photocatalyst [31–34]. The formula is as follows [35]:

$$\ln(C_0/C) = Kt \quad (2)$$

where t is the irradiation time (90 min), C_0/C is the concentration of adsorption–desorption equilibrium after different time intervals, and K is the apparent rate constant (min^{-1}), which is derived from the gradient of the $\ln(C_0/C)$ diagram relative to the time (t). The results show that in Fig. 6, it is clear that all the curves of $\ln(C_0/C)$ versus time (t) are almost linear, the experimental data were fitted to Langmuir, and the R^2 (correlation coefficient) value is as high as 0.9. The rate constants of photocatalytic degradation of MB by blank, nanochains and nanoparticles were

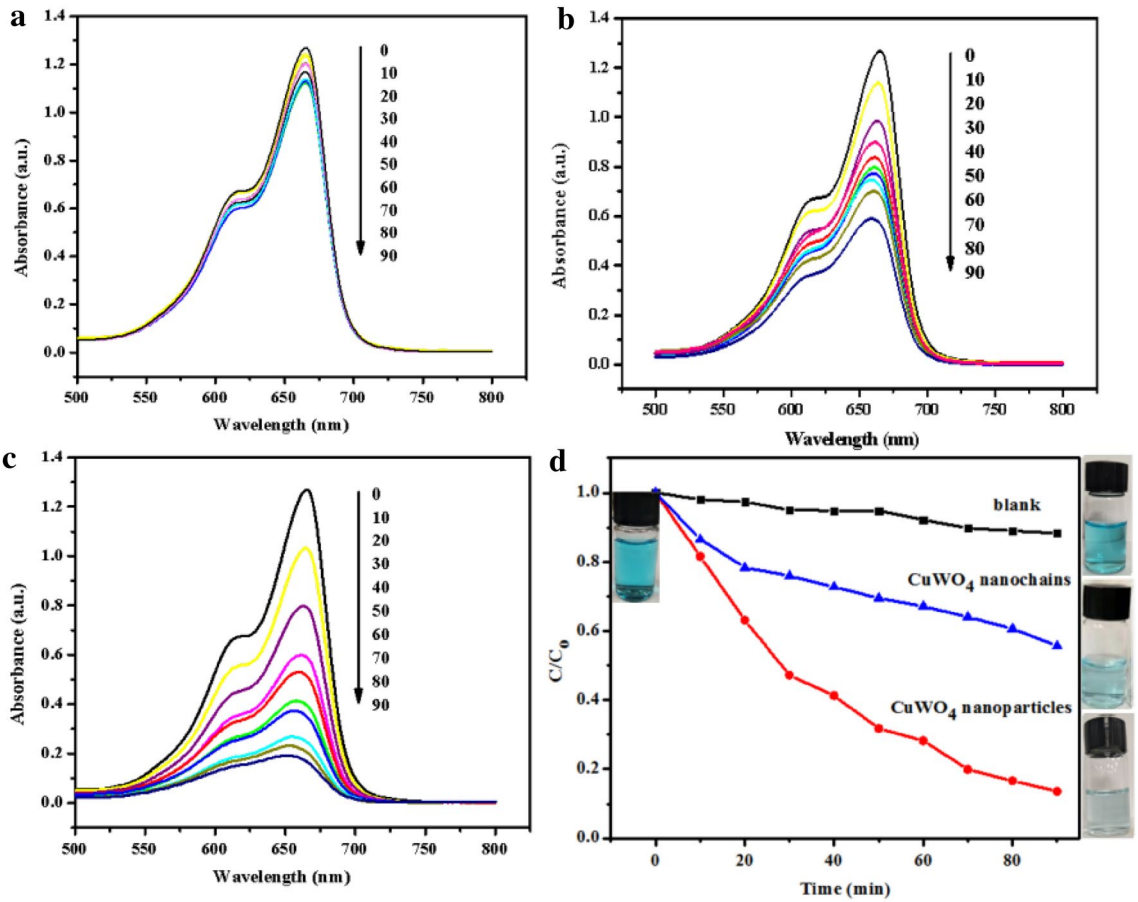

Fig. 5 Absorption spectra of the MB solutions with different degradation time under UV–Vis irradiation for **a** blank; **b** $CuWO_4$ nanochains; **c** $CuWO_4$ nanoparticles; **d** Curves of C/C_0 versus irradiation time and time-dependent photographs of MB solution

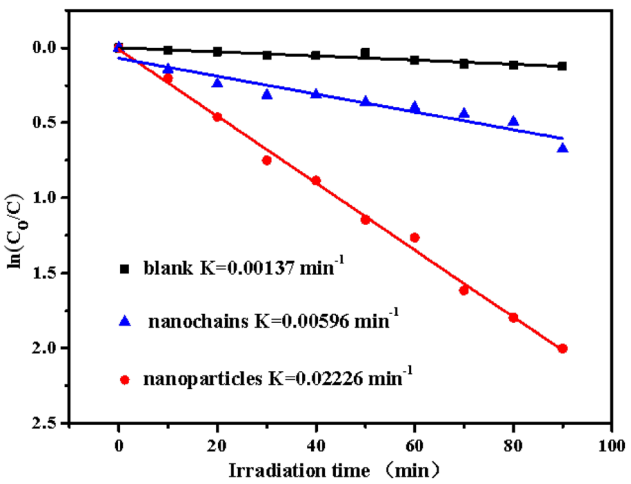

Fig. 6 First-order kinetics data for the UV–Vis photo-degradation of aqueous MB over nanostructured $CuWO_4$

0.00137 min^{-1}, 0.00596 min^{-1} and 0.02226 min^{-1}, respectively. Degradation efficiency under above conditions was found to follow the order of blank < nanochains < nanoparticles. The higher degradation efficiency of $CuWO_4$ nanoparticles may be due to its tremendous properties such as larger surface area, excellent water solubility and high absorbance [36]. The catalyst plays an important role in the whole process of degradation, the morphology of nanoparticles is the best because the nanochains are so heavy that they tend to settle, reducing the likelihood of collisions between molecules.

3.3 Possible mechanism

In principle, $CuWO_4$ nanoparticles were obtained by the reaction between Cu^{2+} and WO_4^{2-} ions as described in Eqs. (3–5):

$$2Na^{+}(aq) + WO_4^{2-}(aq) + 2H_2O + Cu^{2+}(aq) + 2Cl^{-}(aq) + 2H_2O + (CH_2OH)_2 + PVP \xrightarrow[25\,^{\circ}C]{20\,h}$$

$$CuWO_4(amorphous) + 2Na^{+}(aq) + 2Cl^{-}(aq) + 4H_2O + (CH_2OH)_2 + PVP \quad (3)$$

$$CuWO_4(amorphous) \xrightarrow[170\,^{\circ}C]{12\,h} CuWO_4(amorphous) \quad (4)$$

$$CuWO_4(amorphous) \xrightarrow[500\,^{\circ}C]{3.5\,h} CuWO_4(crystalline) \quad (5)$$

Based on the above results, the formation process and growth mechanism of $CuWO_4$ nanochains assembled from nanoparticles are proposed, as shown in Scheme 1. From two aspects of thermodynamics and dynamics, in the beginning, when the saturation of the target solution exceeds the critical value, many tiny $CuWO_4$ crystals nucleate in the solution. With the proceeding of the reaction, when the nucleation size is larger than the critical size, the change value of Gibbs's free energy is greater than the surface energy, and the particles of different sizes are formed in the solution. The surface energy can be adjusted to change the growth rate, the surface free energy of larger particles is smaller compared to that of smaller particles, which increase at a smaller cost. However, according to a typical Ostwald ripening process, the interaction between the growing particles is stronger than the surface active agent [37]. Subsequently, the $CuWO_4$ particles spread and gather together to form tiny $CuWO_4$ nanosheets, because of the magnetic dipole–dipole interaction, these tiny sheets grow into larger nanochains that contribute to the assembly process, that only these main building blocks are linked together rather than results in specific structure directly [38, 39].

In the presence of nanostructured $CuWO_4$ catalyst, the photocatalytic degradation rate of MB is much higher than that of compared to others. It can be deduced that the degradation reaction has changed considerably during the decolorization of organic dye pollutants. As we all know, the photocatalytic activity mainly comes from the photo-induced electrons and holes, and electrons and holes can effectively separate [40, 41]. The electrons and holes produced by photocatalyst have strong redox ability. However, they usually do not react directly with the organic dyes. On the contrary, some active species (such as ·OH and $\cdot O_2^-$) are formed through the reaction of H_2O or O_2 by charge and absorption [42, 43]. It is well learned that holes (h^+), hydroxyl radicals (·OH) and superoxide anion radical ($\cdot O_2^-$) are regarded as the reactive species of photocatalytic reaction [44]. When the $CuWO_4$ samples were irradiated by UV–Vis light with the energy of higher or equal than it is band gap energy ($h\upsilon \geq Eg$), the photo generated electrons were induced in the conduction band, and holes were induced in the valence band and water oxidation reduction potentials. The specific schematic for degradation of MB over $CuWO_4$ photocatalyst was shown in Scheme 2 and the mechanism of photocatalysis for degradation of MB is proposed as follows:

$$CuWO_4 + h\upsilon \rightarrow CuWO_4(e_{CB}^- + h_{VB}^+) \quad (6)$$

$$e_{CB}^- + O_2 \rightarrow \cdot O_2^- \quad (7)$$

$$h_{VB}^+ + H_2O \rightarrow H^+ + OH\cdot \quad (8)$$

$$h_{VB}^+ + OH^- \rightarrow OH\cdot \quad (9)$$

$$H_2O + \cdot O_2^- \rightarrow O_2H\cdot + OH^- \quad (10)$$

$$2O_2H\cdot \rightarrow O_2 + H_2O_2 \quad (11)$$

$$H_2O_2 \rightarrow 2OH\cdot \quad (12)$$

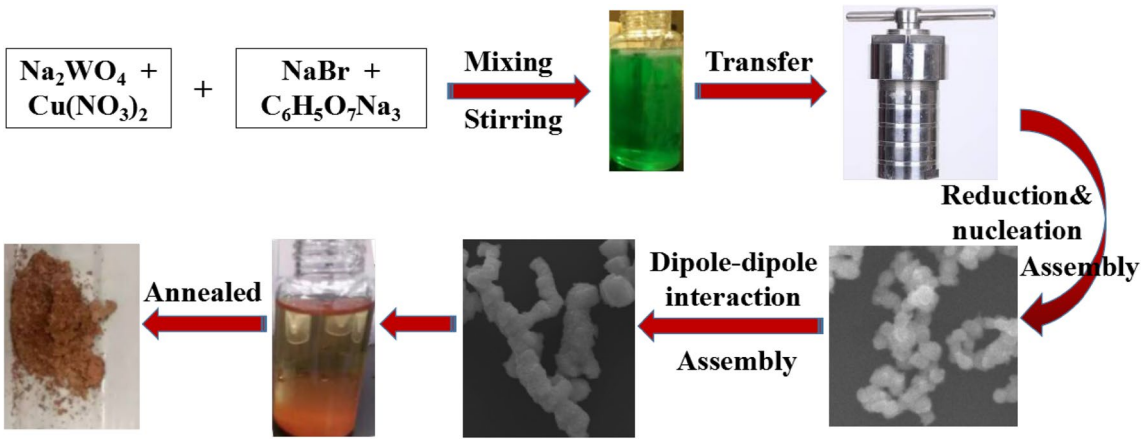

Scheme 1 Schematic representation of the formation process for the $CuWO_4$ nanochains

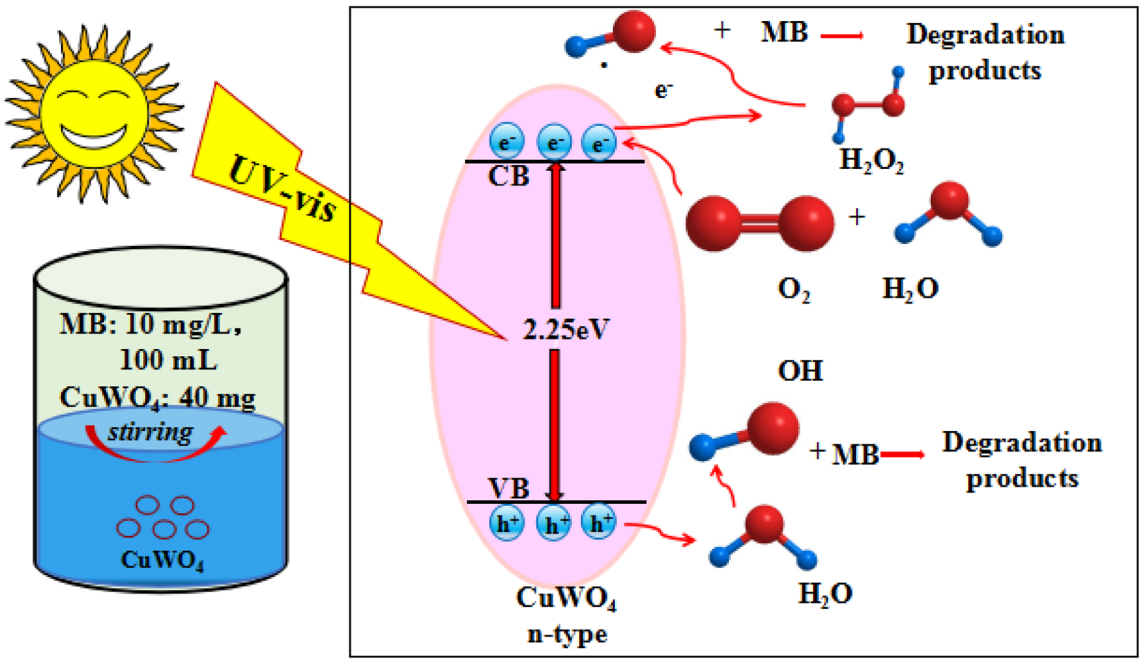

Scheme 2 Reaction mechanism of MB photo-degradation over $CuWO_4$ under UV–Vis light irradiation

$$OH \cdot + MB \rightarrow \text{degradation products} \quad (13)$$

$$\cdot O_2^- + MB \rightarrow \text{degradation products} \quad (14)$$

The results demonstrated that the $CuWO_4$ nanomaterials may have high photocatalytic activity for remove of organic compounds from waste water under irradiation of UV–Vis light. Besides, on the basis of mechanism, OH·, O_2H·, $\cdot O_2^-$ and H_2O_2 play an important role in degradation process, if H_2O_2 is added into the aqueous solution of MB, it can promote the separation of excited carriers under illumination. In addition, the smaller particles can ensure better contact between atoms and a greater chance of collision, which is conducive to the reaction and the separation of photo generated electron–hole pairs. This proposal has given directions for future work and improvements.

4 Conclusions

In summary, the photocatalytic activity of $CuWO_4$ was studied to assess their ability to depurate water streams efficiently from organic pollutants, such as MB. Here, $CuWO_4$ nanoparticles have been synthesized through the solvothermal method, the nanoparticles sample has better degradation MB ability than nanochains. 86% MB were degraded by employing nanoparticles as photocatalyst after 90 min under irradiation of UV–Vis light, while the nanochains sample only degraded by 49%. In addition, it is demonstrated that the shape and size of materials have an impact on the photocatalytic activity of $CuWO_4$, which follows the first order kinetic mechanism. By adjusting their size from a kinetic and thermodynamic perspective, the band gap of the material can be adjusted, the smaller the nanoparticles, the higher the frequency of absorption wavelengths. Our results indicated that the $CuWO_4$ nanomaterials are potential materials for photocatalytic degradations of MB.

Acknowledgements This work was supported by the fundamental research funds for the Central Universities (No. 106112015CDJZR305501).

Compliance with ethical standards

Conflict of interest The authors declare no competing financial interest.

References

1. Barzgari Z, Askari SZ, Ghazizadeh A (2017) Fabrication of nanostructured $CuWO_4$ for photocatalytic degradation of organic pollutants in aqueous solution. J Mater Sci Mater Electron 28:3293–3298
2. Youngblood WJ, Lee SA, Maeda K, Mallouk TE (2009) Visible light water splitting using dye-sensitized oxide semiconductors. Acc Chem Res 42:1966–1973

3. Zhang X, Veikko U, Mao J, Cai P, Peng T (2012) Visible-light-induced photocatalytic hydrogen production over binuclear rull-bipyridyl dye-sensitized TiO_2 without noble-metal loading. Chem Eur J 18:12103–12111
4. Manavi N, Kazemi AS, Bonakdarpour B (2017) The development of aerobic grannules from conventional activated sludge under anaerobic-aerobic cycles and their adaptation for treatment of dyeing wastewater. Chem Eng J 312:315–384
5. Schwarzenbach R, Escher BI, Fenner K, Hofstetter TB, Johnson CA, von Gunten U, Wehrli B (2006) The challenge of micripollutants in aquatic systems. Science 313:1072–1077
6. Yan J, Wang K, Xu H, Qian J, Liu W, Yang X, Li H (2013) Visible-light photocatalytic efficiencies and anti-photocorrosion behavior of CdS/graphene nanocomposites: evaluation using methylene blue degradation. Chin J Catal 34:1876–1882
7. Hou X, Li Y, Wang C (2014) Highly efficient photocatalysis of p-type Cu_2ZnSnS_4 under visible-light illumination. Mater Res Bull 60:628–633
8. Pirhashemi M, Habibi-Yangjeh A (2015) Ternary ZnO/$AgCrO_4$ nanocomposites with tandem n–n heterojunctions as novel visible-light-driven photocatalysts with excellent activity. Ceram Int 41:14383–14393
9. Siriwong P, Thongtem T, Phuruangrat A, Thongtem S (2011) Hydrothermal synthesis, characterization, and optical properties of wolframite ZnWO4 nanorods. Cryst Eng Commun 13:1564–1569
10. Zawawi SMM, Yahya R, Hassan A, Mahmud HNME, Daud MN (2013) Structural and optical characterization of metal tungstates (MWO_4; M = Ni, Ba, Bi) synthesized by a sucrose-templated method. Chem Cent J 7:80–90
11. Naderi HR, Sobhani-Nasab A, Rahimi-Nasrabadi M, Ganjali MR (2017) Decoration of nitrogen-doped reduced graphene oxide with cobalt tungstate nanoparticles for use in high-performance supercapacitors. Appl Surf Sci 423:1025–1034
12. Zhang J, Wang Y, Li S, Wang X, Huang F, Xie A, Shen Y (2011) Controlled synthesis, growth mechanism and optical properties of $FeWO_4$ hierarchnical microstructures. Cryst Eng Commun 13:5744–5750
13. Almedia MAP, Cavalcante LS, Li MS, Varela JA, Longo E (2012) Structure refinement and photoluminescence properties of $MnWO_4$ nanorodes obtained by microwave-hydrothermal synthesis. J Inorg Organomet Polym 22:264–271
14. Jovanovic DJ, Validzic Lj I, Mitric M, Nedeljkovic JM (2012) Synthesis and structural characterization of nano-sized copper tungstate particles. Acta Chim Slov 59:70–74
15. Muthamizh S, Suresh R, Giribabu K, Manigandan R, Kumar SP, Munusamy S, Vijayalakshmi L, Stephen A, Narayanan V (2014) Solid state synthesis of copper tungstate nanoparticles and its electrochemical detection of 5-chlorophenol. AIP Conf Proc 1591:508–510
16. Yourey JE, Bartlett BM (2011) Electrochemical deposition and photoelectrochemistry of $CuWO_4$, a promising photoanode for water oxidation. J Mater Chem 21:7651–7660
17. Errandonea D, Manjon FJ (2008) Pressure effects on the structural and electronic properties of ABX_4 scintillating crystals. Prog Mater Sci 53:711–773
18. Ruiz-Fuertes J, Errandonea D, Segura A, Manjon FJ, Zhu Zh, Tu CY (2008) Growth, characterization, and high-pressure optical studies of $CuWO_4$. High Press Res 28(4):565–570
19. Chang Y, Braun A, Deangelis A, Kaneshiro J, Gaillard N (2011) Effect of thermal treatment on the crystallographic, surface energetics, and photoelectrochemical properties of reactively cosputtered copper tungstate for water splitting. J Phys Chem C 115:25490–25495
20. Kunz M, Brown ID (1995) Out-of-center distortions around octahedrally coordinated d^0 transition metals. J Solid State Chem 115:395–406
21. Ruiz-Fuertes J, Friedrich A, Pellicer-Porres J, Errandonea D, Segura A, Morgenroth W (2011) Structure solution of the high-pressure phase of $CuWO_4$ and evolution of the Jahn–Teller distortion. Chem Mater 23:4220–4226
22. Ruiz-Fuertes J, Segura A, Rodríguez F, Errandonea D, Sanz-Ortiz MN (2012) Anomalous high-pressure Jahn–Teller behavior in $CuWO_4$. Phys Rev Lett 108:166402
23. Timoshenko J, Anspoks A, Kalinko A, Kuzmin A (2015) Local structure of nonosized tungstates revealed by evolutionary algorithm. Phys Status Solidi (a) 212:265–273
24. Kihlborg L, Gebert E (1970) $CuWO_4$, a distorted wolframite-type structure. Acta Crystallogr Sec B 26:1020–1025
25. Rietveld HM (1969) A profile refinement method for method for nuclear and magnetic structures. J Appl Crystallogr 2:65–71
26. Schofield PF, Knight KS, Redfern SAT, Cressey G (1997) Distortion characteristics across the structural phase transition in (Cu1–xZnx)WO_4. Acta Crystallogr B 53:102–112
27. Souza ELS, Dalmaschio CJ, Filho MGR (2014) Structural refinement and photocatalytic properties of $CuWO_4$ crystals. Microsc Adv Sci Res Educ 2:894–902
28. Wang YW, Cheng HB, Zhu ZL (2005) Structure and vibration spectrum of laser crystal Yb: KGd (WO). J Inorg Mater 20:1295–1300
29. Mancheva MN, Iordanova RS, Klissurski DG (2007) Direct mechanochemical synthesis of nanocrystalline $NiWO_4$. J Phys Chem C 111:1101–1104
30. Dashamiri S, Ghaedi M, Dashtian K, Rahimi MR, Goudarzi A, Jannesar R (2016) Ultrasonic enhancement of the simultaneous removal of quaternary toxic organic dyes by CuO nanoparticles loaded on activated carbon: central composite design, kinetic and isotherm study. Ultrason Sonochem 31:546–557
31. Mohapatra L, Parida K, Satpathy M (2012) Molybdate/tungstate intercalated oxo-bridged Zn/Y LDH for solar light induced photodegradation of organic pollutants. J Phys Chem C 116:13063–13070
32. Dong X, Ding W, Zhang X, Liang X (2007) Mecharism and kinetics model of degradation of synthetic dyes by UV–Vis/H_2O_2/ferrioxalate complexes. Dyes Pigments 74:470–476
33. Zhang L, Yang H, Xie X, Zhang F, Li L (2009) Preparation and photocatalytic activity of hollow ZnSe microspheres via ostwald ripening. J Alloy Compd 473:65–70
34. Sarkar D, Maiti UN, Ghosh CK, Chattopadhyay KK (2012) Excellent photocatalytic activity of mixed phase ultra slim TiO_2 nanofibers for the degradation of organic wastes. Adv Sci Lett 6:127–133
35. Li Y, Li X, Li J, Yin J (2006) Photocatalytic degradation of methyl orange by TiO_2-coated activated carbon and kinetic study. Water Res 40:1119–1126
36. Gao B, Fan H, Zhang X, Song L (2012) Template-free hydrothermal synthesis and high photocatalytic activity of $ZnWO_4$ nanorods. Mater Sci Eng, B 177:1126–1132
37. Roosen AR, Carter WC (1998) Simulations of microstructural evolution: anisotropic growth and coarsening. Phys A 261:232–247
38. Vandewalle N, Ausloos M (1997) Construction and properties of fractal trees with tunable dimension: the interplay of geometry and physics. Phys Rev E 55:94
39. Zhu LP, Xiao HM, Fu SY (2007) Surfactant-assisted synthesis and characterization of novel chain-like CoNi alloy assemblies. Eur J Inorg Chem 25:3947–3951
40. Li N, Liu G, Zhen C, Li F, Zhang L, Cheng H (2011) Battery performance and photocatalytic activity of mesoporous anatase

TiO_2 nanospheres/graphene composites by template-free self-assembly. Adv Funct Mater 21:1717–1722
41. Li T, He Y, Lin H, Cai J, Dong L, Wang X, Luo M, Zhao L, Yi X, Weng W (2013) Synthesis, characterization and photocatalytic activity of visible-light plasmonic photocatalyst AgBr–$SmVO_4$. Appl Catal B Environ 138–139:95–103
42. Li J, Cai S, Xu Z, Chen X, Jia H, Chen J (2017) Solvothermal syntheses of Bi and Zn co-doped TiO_2 with enhanced electron-hole separation and efficient photode gradation of gaseous toluene under visible-light. J Hazard Mater 325:261–270
43. Cao J, Xu B, Luo B, Lin H, Chen S (2011) Preparation, characterization and visible-light photocatalytic activity of Ag/AgCl/TiO_2. Appl Surf Sci 257:7083–7089
44. Etacheri V, Di Valentin C, Schneider J, Bahnemann D, Pillai SC (2015) Visible-light activation of TiO_2 photocatalysts: advances in theroy and ecperments. J Photochem Photobiol C Photochem Rev 25:1–29